A Self-Consistency Approach to Improve Microwave Rainfall Rate Estimation from Space

CHRISTIAN KUMMEROW

Universities Space Research Association, USRA Visiting Scientist Program, Goddard Space Flight Center, Greenbelt, Maryland

ROBERT A. MACK AND IDA M. HAKKARINEN

General Sciences Corporation, Laurel, Maryland

(Manuscript received 24 May 1988, in final form 20 January 1989)

ABSTRACT

A multichannel statistical approach is used to retrieve rainfall rates from brightness temperatures (T_B's) observed by passive microwave radiometers flown on a high-altitude NASA aircraft. Brightness temperature statistics are based upon data generated by a cloud radiative model. This model simulates variabilities in the underlying geophysical parameters of interest, and computes their associated T_B's in each of the available channels. By further imposing the requirement that the observed T_B's agree with the T_B values corresponding to the retrieved parameters through the cloud radiative transfer model, the results can be made to agree quite well with coincident radar-derived rainfall rates. Some information regarding the cloud vertical structure is also obtained by such an added requirement.

The applicability of this technique to satellite retrievals is also investigated. Data which might be observed by satellite-borne radiometers, including the effects of nonuniformly filled footprints, are simulated by the cloud radiative model for this purpose. Results from statistics generated using different hydrometeor vertical profiles in the cloud radiative model are examined. It is found that errors in the retrieved rainfall rates, and retrieval biases, decrease with increasing agreement between simulated T_B's and those corresponding to the retrieved geophysical parameters.

1. Introduction

Passive microwave techniques for the estimation of rainfall have advanced considerably over the past few years, due largely to an increased understanding of the transfer of microwave radiation through precipitating clouds. Cloud radiative models, such as those by Weinman and Guetter (1977), Wilheit et al. (1982), Wu and Weinman (1984), Szejwach et al. (1986), Olson (1987) and Kummerow and Weinman (1988), have all been used extensively to study the sensitivity of microwave brightness temperatures (T_B's) to variations in atmospheric and precipitation parameters. Cloud microphysical models (e.g., Tao and Simpson 1984; Tao et al. 1987) have meanwhile contributed to a better understanding of the vertical profile of liquid and frozen hydrometeors in precipitating clouds. It is found that, in addition to the rain rate and the portion of the radiometer footprint covered by rain, the microwave T_B's depend upon several other factors. The most significant of these are: nonprecipitating cloud droplets, vertical distribution of liquid and frozen drops, drop-size distributions and surface characteristics. Furthermore, the relative importance of these parameters depends upon both the nature of the precipitating cloud and the microwave frequency being used for observation.

Multifrequency data, in conjunction with information relating the observed T_B's at each frequency to cloud constituents and surface characteristics, are needed in order to retrieve rainfall in the presence of the above-mentioned variables. Although a real atmosphere contains many more free parameters than can realistically be retrieved using microwave data, it is nonetheless possible to retrieve rainfall rates by focusing upon the parameters which most influence the upwelling brightness temperatures.

This study uses a multifrequency piecewise-linear regression technique (Kummerow 1987) to interpret observed T_B's in terms of rainfall rates. In the absence of detailed measurements, regression statistics are generated by a cloud radiative model. A cloud radiative model, in the present context, consists of a complete description of the atmospheric parameters, cloud constituents and surface characteristics needed to perform radiative transfer calculations. The free variables of such a cloud radiative model are further defined as those variables which are to be retrieved. The surface rainfall rate, for instance, is allowed to take on all possible values from 0 to 100 mm h^{-1} in generating statistics. Similarly, the surface temperature and nonpre-

Corresponding author address: Dr. C. Kummerow, Code 612, Goddard Space Flight Center, Greenbelt, MD 20771.

cipitating cloud water are generally allowed to take on all possible values within some reasonable range. The specific choice of quantities which are to be varied freely, as mentioned earlier, is generally dictated by our a priori knowledge of the dependence of brightness temperatures on various quantities for different types of precipitation (i.e., stratiform or convective rain).

The quantities of secondary importance in determining upwelling brightness temperatures, such as the ice parameterization for light precipitation, or the cloud water in heavy precipitation, are incorporated as unknown parameters into the cloud radiative model. Although unknown, these parameters must nonetheless be specified in order to generate regression statistics. Previous experience, alternate data sources, cloud microphysical models or climatological information can be used to make these assumptions as realistic as possible.

Regression statistics obtained from such a cloud radiative model are subject to many errors stemming from the often arbitrary values assigned to the unknown parameters in such models. Improvements in statistical methods of rainfall estimation, therefore, depend critically on the correct understanding and modeling of the rain scene. By requiring consistency between observed T_B's and those calculated from the cloud radiative model at each frequency for a given set of retrieved parameters, it appears possible to adjust the cloud radiative model parameters to specific rain conditions. The results obtained in this fashion are correspondingly in very good agreement with simultaneous radar observations. The skill of such a technique is demonstrated for high resolution aircraft data obtained during the COoperative Huntsville Meteorological EXperiment (COHMEX) (Dodge et al. 1986), conducted during the summer of 1986. Simulated satellite data are used to show how this technique might be adapted to interpret satellite microwave observations such as those from the Special Sensor Microwave/Imager (SSM/I), or the proposed Tropical Rainfall Measurement Mission (TRMM).

2. Retrieval algorithm

The most direct approach for deducing geophysical parameters is to rely upon previous brightness temperature measurements, along with their observed geophysical parameters, to interpret data. Spencer (1986) has had success applying such an empirical technique to 37 GHz observations over the Gulf of Mexico from the Scanning Multichannel Microwave Radiometer (SMMR) on the Nimbus-7 satellite. Such a technique works well if the representative dataset is relatively homogeneous. If it is heterogeneous, then such a technique would require a large number of satellite observations along with coincident ground truth data over all the distinct world regions and climates. These data are often either nonexistent or very costly to obtain.

An alternate approach which does not suffer from these shortcomings is to use one of the cloud radiative models mentioned earlier to create large datasets relating the rainfall rate and other geophysical parameters of interest to microwave brightness temperatures. Multiple linear regression methods may then be applied to these data in order to obtain regression coefficients relating the geophysical parameters of interest (i.e., surface rainfall rate) to a linear combination of the observed brightness temperatures. This can be expressed as

$$R = a_0 + \sum_{i=1}^{N} a_i T_{Bi} \qquad (1)$$

where R is the surface rainfall rate in mm h^{-1}, N is the total number of available channels, a_0 and a_i are the regression coefficients and T_{Bi} are the brightness temperatures for each channel i, respectively.

The form of Eq. (1) suggests that a good fit to any brightness temperature dataset might be achieved if the relationship between it and the geophysical parameter is linear. Unfortunately, the surface rainfall rate, which is the parameter of greatest interest in this study, is known to be a highly nonlinear function of the brightness temperature. This obstacle is overcome by performing separate regression analyses over six rainfall rate intervals: 0–3 mm h^{-1}, 3–6 mm h^{-1}, 6–10 mm h^{-1}, 10–20 mm h^{-1}, 20–40 mm h^{-1} and 40–100 mm h^{-1}. Over these intervals, the rainfall rate is approximately a linear function of the brightness temperature at each microwave frequency. For simplicity, regression analyses for the remainder of the geophysical parameters are also performed over these intervals.

In the foregoing development, separate regression coefficients are produced for each of the six rainfall rate intervals. Thus, a method for identifying the correct interval must be included in the inversion procedure. This is accomplished by first estimating the rainfall rate based upon the brightness temperature of a single channel. The regression coefficients corresponding to this interval are then used to calculate the retrieved rainfall rate. If this retrieved rainfall rate lies within the same interval as the initial estimate, then the procedure is said to have converged and the remaining parameters are calculated using regression coefficients from that interval. If the calculated rainfall rate falls in some interval other than the one selected by the initial estimate, then this new interval is used as an initial estimate, and the procedure is repeated until convergence is achieved.

Good results for rainfall rate retrievals have been obtained using piecewise-linear statistical procedures on simulated data. Chang and Milman (1982) were able to simultaneously retrieve rain rate, as well as the ocean surface temperature, surface wind speed and cloud liquid water to within 10% using a scheme very similar to this. Kummerow (1987), using the above procedure, was able to obtain accuracies of 20% for

rainfall rates over both land and water, assuming random distributions of surface temperature and cloud liquid water contents, as well as cloud dimensions and cloud locations, within the radiometer footprint. Accuracies for retrievals such as these, however, are often artificially high because such studies rely upon the same cloud radiative model to simulate satellite observations and to generate data for the regression analyses. This, as will be shown later, is an idealized situation which assumes complete knowledge of the cloud structure and radiative processes, and generally produces much better results than are possible with actual observations.

The cloud radiative model, as described earlier, contains a limited number of free variables (i.e., rainfall rate, cloud water, surface temperature and emissivity) which are varied randomly to generate retrieval statistics. The selection of cloud radiative model parameters, however, are often subject to uncertainties. In order to avoid errors which can be introduced by making incorrect assumptions in the cloud radiative model, the present retrieval technique relies upon a feedback mechanism to evaluate the performance of the model. The process is diagrammed in Fig. 1. It is clear that, if the cloud radiative model accurately represents the underlying rain scene, then it will generate multifrequency sets of brightness temperatures which are very similar in nature to the observed T_B's. This, in turn, produces retrieved quantities whose corresponding brightness temperatures closely resemble the observations. The converse of this statement, however, is true only if a given set of brightness temperatures can be shown to correspond to a unique set of geophysical parameters. Although no proof of uniqueness is given here, it is felt that good results can be obtained as long as the total number of independent channels exceeds the number of variables (free and parameterized) needed to adequately describe a given rain scene.

3. The cloud radiative model

Over the radiometrically cold ocean, low frequency (<20 GHz) microwave T_B's tend to increase with rainfall rate due to the thermal emission of raindrops and cloud water. Recent satellite missions such as the Defense Meteorological Satellite Program (DMSP), however, have turned to higher frequency microwave channels that measure scattering effects produced by large raindrops and ice. The brightness temperature depressions produced by these scattering events are advantageous because they can be interpreted over both oceans and radiometrically warm land. Higher frequencies (37 and 85.6 GHz) are also advantageous because they are very sensitive to low rainfall rates over water, and they have smaller footprints, effectively reducing the error associated with inhomogeneities within the raining cloud. The disadvantage of these high frequencies is that the signal will be most sensitive to the upper layers of the precipitating cloud (Huang and Liou 1983; Wu and Weinman 1984). This is due to the strong attenuation produced by the scattering of ice and large raindrops. Thus, although these high frequencies provide the potential to infer precipitation over both water and land, they also make it necessary to parameterize much of the cloud vertical structure, such as the relation between the ice aloft and the underlying rainfall, as well as the cloud liquid water distribution.

Recent work by Adler et al. (1988a) has shown that averaging of high spatial resolution brightness temperatures over large areas tends to reduce variations in the relationships between T_B's and surface rainfall rate. Inversely, if the field of view is diminished, then the variations in cloud parameters tend to make the brightness temperatures very sensitive functions of the cloud structure. Proposed satellite missions such as TRMM (Simpson et al. 1988), with unprecedented small fields of view (10 × 10 km), will therefore be even more sensitive to the parameterization of the cloud properties within the radiometer footprint. The cloud radiative model must therefore have two qualities: it must be simple enough not to overwhelm the retrieval procedure with unnecessary detail, yet complex enough to allow for the adequate representation of various cloud vertical hydrometeor profiles. The cloud radiative model which most closely meets the above specifications was thought to be an Eddington type solution containing five independent vertical layers. The Eddington solution is advantageous because it accounts for multiple scattering while remaining computationally very efficient. Finite cloud effects can also be dealt with, in a first approximation, following the procedure described by Kummerow and Weinman (1988). The five vertical layers were thought to be the minimum number of layers required to adequately describe the hydrometeor profiles observed in this study. Figure 2 shows how the cloud constituents are distributed in the five layers. Nonprecipitating cloud water or ice consists of particles which have not attained the necessary size to fall as precipitation. Due to their small size, these constituents are assumed not to scatter radiation. The thickness and the liquid water/ice content of each layer can be specified independently. This allows for the accurate representation of most cloud hydrometeor profiles.

The hydrometeors are assumed to follow a Marshall and Palmer (1948) drop-size distribution. In order to account for observed differences in the horizontal and vertical polarizations at high rainfall rates (Spencer et al. 1983), this model further assumes the hydrometeors (both liquid and ice) to be oblate spheroids whose shape is given by

$$\frac{a}{b} = 1 - 0.92r \tag{2}$$

where a and b are the semimajor and semiminor axes of the spheroid, respectively, and r is the equivalent

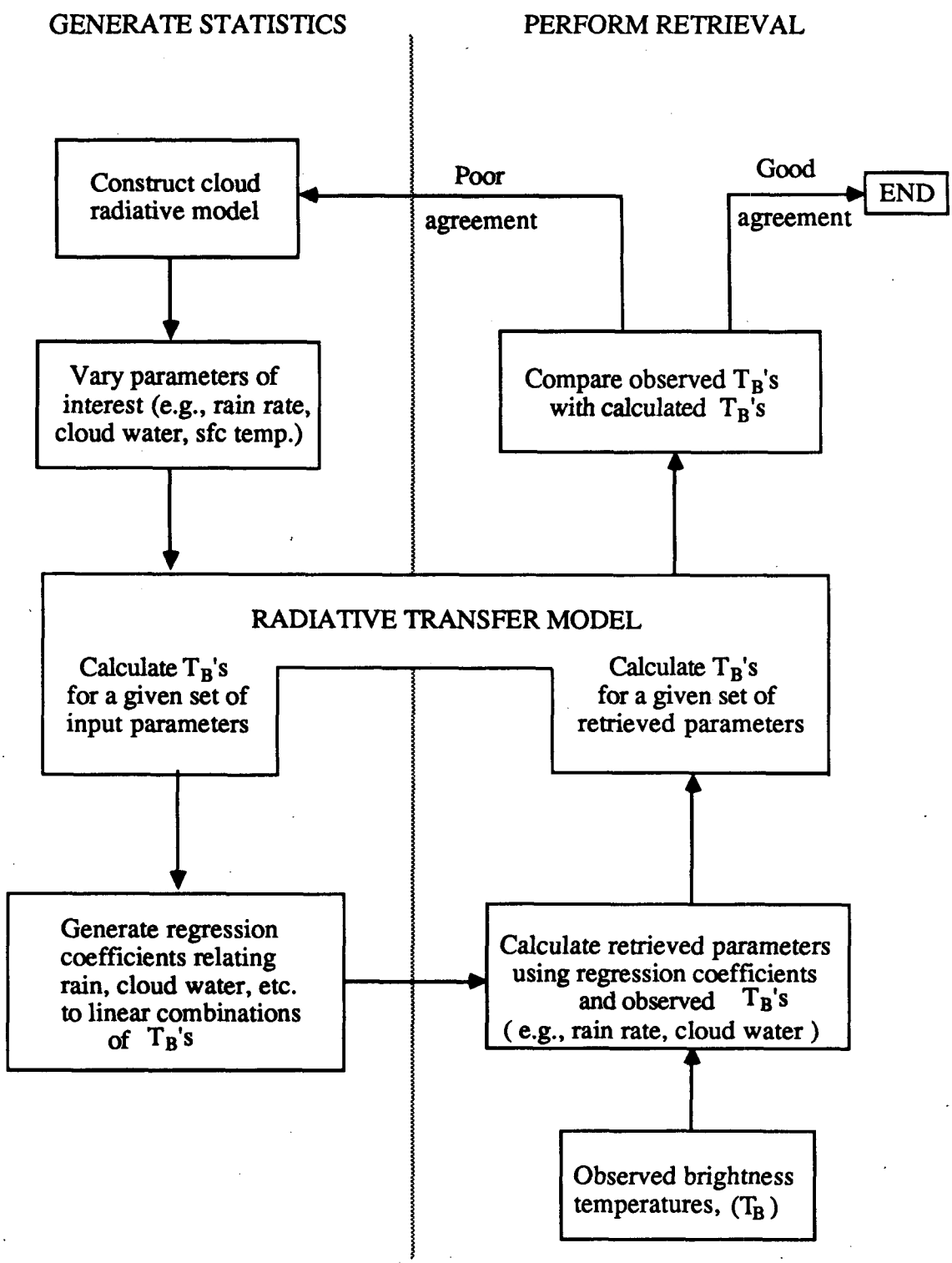

FIG. 1. Flow chart showing the iterative procedure used to adjust the cloud radiative model parameters to the underlying rainfall scene.

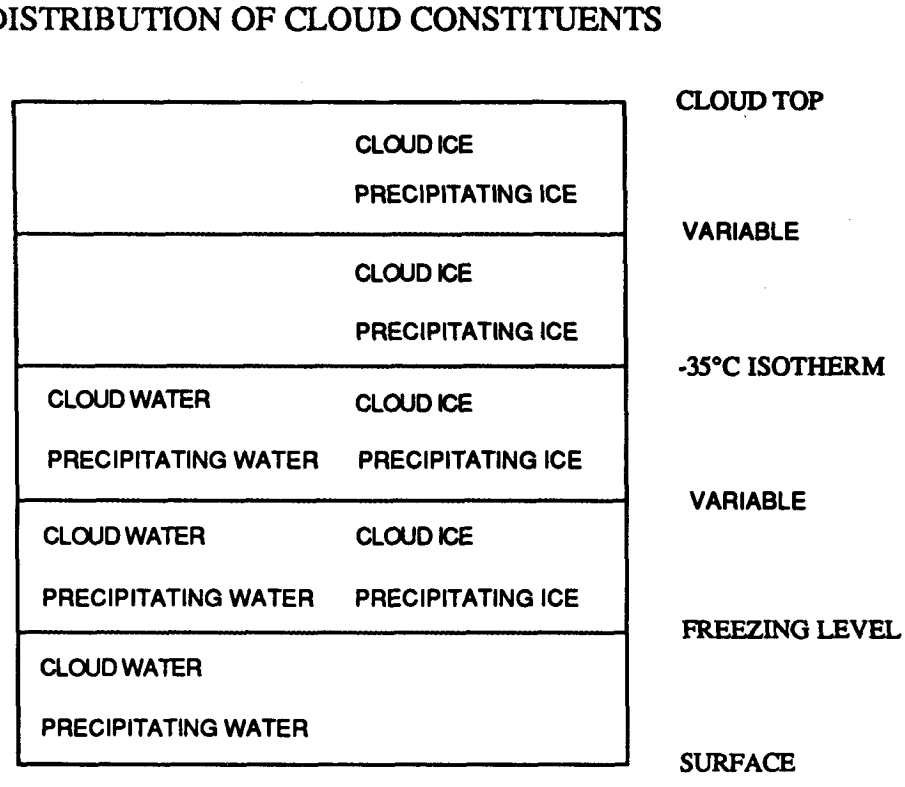

FIG. 2. Vertical distribution of cloud constituents in the five layer cloud model. Only the indicated constituents are allowed to exist in each of the five layers.

radius in mm prescribed by the Marshall–Palmer drop-size distribution. Such a shape assumption was also used by Oguchi (1983) and Evans and Holt (1977) to explain depolarization effects in satellite communication links due to the presence of liquid and frozen hydrometeors, respectively. Although such spheroidal particles are likely to be poor representations of the shape of individual ice particles, this simplified shape appears to be a good representation for an ensemble of particles when radiation is scattered numerous times, as in traversing optically thick clouds. The same argument shows that the brightness temperatures are not affected significantly by this shape assumption for optically thin (low rainfall rate) clouds.

4. Case studies

COHMEX provided a unique dataset consisting of high spatial resolution radiometric measurements from a NASA high-altitude ER-2 aircraft with coincident ground truth measurements provided by well-calibrated surface radars. The microwave instrumentation on the ER-2 aircraft consisted of the Microwave Precipitation Radiometer (MPR) measuring 18 and 37 GHz brightness temperatures, and the Advanced Microwave Moisture Sounder (AMMS), which observed at 92 and 183 GHz. The MPR pointed ahead of the aircraft at 45°, measuring both horizontal and vertical polarization, while the AMMS scanned directly beneath the aircraft across nadir. At a nominal altitude of 20 km, the ground resolution for the MPR channels was ~3 km, while the 92 GHz channel resolution was ~0.7 km. The 183 GHz information was not used in this study.

The ER-2 aircraft flew two special missions during COHMEX within range of NASA's SPANDAR radar at Wallops Island, Virginia. The first case to be presented was on 1 July 1986, when the aircraft overflew light stratiform rain over the ocean. The second case was on 29 June 1986, when the aircraft made two passes over deep convection with intense rainfall along the North Carolina–Virginia border. Preliminary data analysis on this case was conducted by Adler et al. (1988b).

a. Stratiform rain case—1 July 1986

On 1 July 1986, the NASA aircraft overflew light stratiform precipitation off the coast of the Delmarva peninsula near Wallops Island, Virginia. Brightness temperatures measured by the MPR during a flight line from 1643–1658 UTC are shown in Fig. 3. Since the flight line is over the radiometrically cold ocean, rainfall is characterized by warmer T_B values associated with the thermal emission of raindrops. Two rain areas are apparent in this flight line: from 20 to 80 km (1644:30–1649:00 UTC) along the flight path is a broad region of increased microwave T_B, and between 90

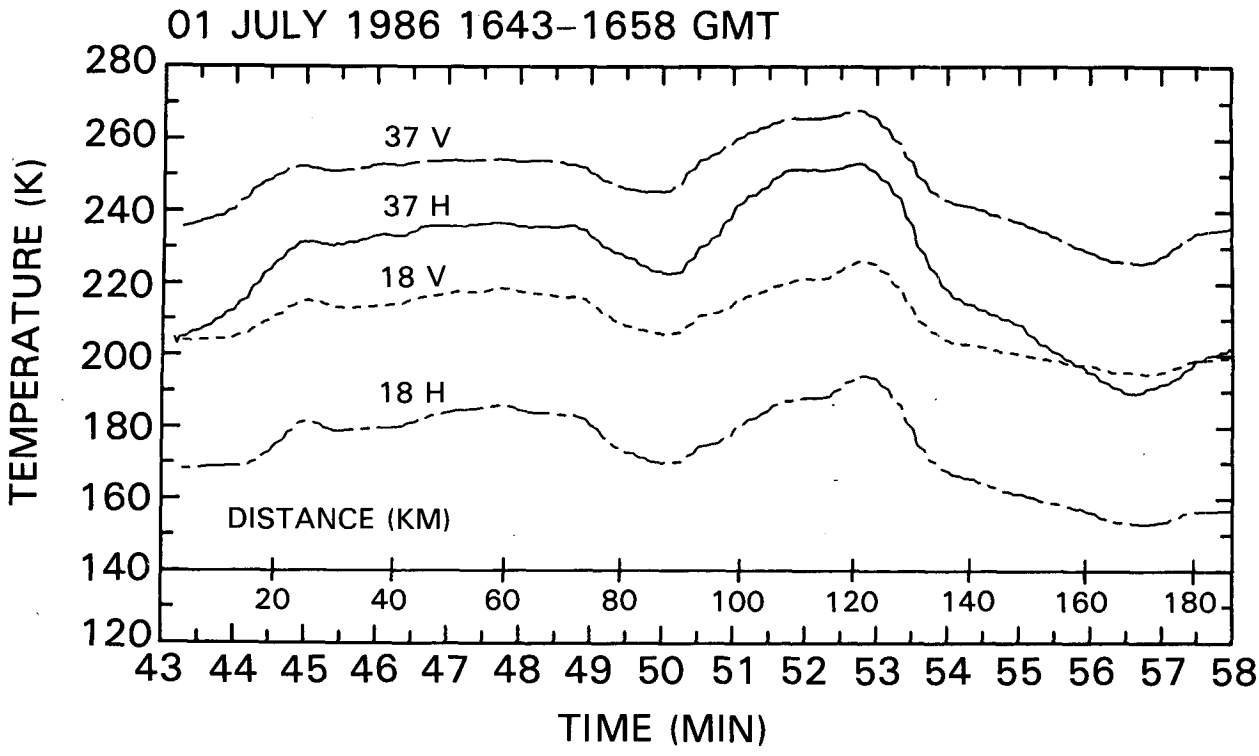

FIG. 3. Traces of the MPR brightness temperature measurements as a function of time as the aircraft overflew precipitation over water off the coast of Virginia on 1 July 1986. The distance scale refers to the horizontal distance of the aircraft from the radar at Wallops Island, Virginia.

and 130 km (1650:00–1653:30 UTC) is a narrower, but higher peak in the T_B's.

The NASA SPANDAR radar was scanning in range-height indicator (RHI) mode at this time in order to collect data along the vertical plane defined by the aircraft track as the plane flew along the 120° radial. Figure 4a shows the rainfall rates derived from the vertical scan made during 1645–1646 UTC. Radar reflectivity was converted to rainfall rate by assuming a Marshall–Palmer drop-size distribution. Below the freezing level (4 km), the rain rate–reflectivity relation is given by

$$R = \left(\frac{Z}{200}\right)^{0.625} \tag{3}$$

where R is the rain rate in mm h^{-1} and Z is the equivalent radar reflectivity in $mm^6 \cdot m^{-3}$. To account for the lower reflectivity of the ice above the freezing level, 7 dBZ were added to the reflectivities measured above 4 km (Smith 1984). This adjustment results in rain rates for ice which are 2.7 times higher than the rain rates for liquid of a given reflectivity. The narrow strip of artificially high rain rates at ~4 km is a result of the "bright band" effect, caused by the increased reflectivity of melting ice particles falling through the freezing level. The bright band is frequently found in light precipitation situations (Ramana Murty et al. 1965).

Figure 4b shows the retrieved surface rainfall rate using the four channels of the MPR. (The 92 GHz data were examined, but not used as input for the retrieval scheme.) A nominal aircraft altitude of 20 km was assumed to determine the position of the surface rainfall to account for the 45° forward-viewing geometry of the MPR instrument. This allows direct comparison between radar-derived and aircraft sensor-derived rainfall rates.

For this retrieval, hydrometeors were distributed in the lowest two of the five available layers in the cloud radiative model. The layer which extends from the surface to the freezing level (4 km) was assumed to contain a uniform rainfall rate, R_L, and cloud liquid water, Q_L. The layer above the freezing level was initially assumed to be 2 km thick, to consist of ice particles, and to have an ice water content (IWC) of $0.5 \cdot R_L$. This last assumption is quite arbitrary and is meant only as a first guess to the cloud vertical structure. The remaining three layers of the cloud radiative model were assigned absorption properties of the U.S. Standard Atmosphere.

Statistics were generated by varying R_L, Q_L, the ocean surface temperature, T_S, and the surface wind speed, U_0, which is related to the surface roughness and thus the emissivity of the surface. Since the rain rate was known to be light from both the behavior of the brightness temperatures, as well as the radar image,

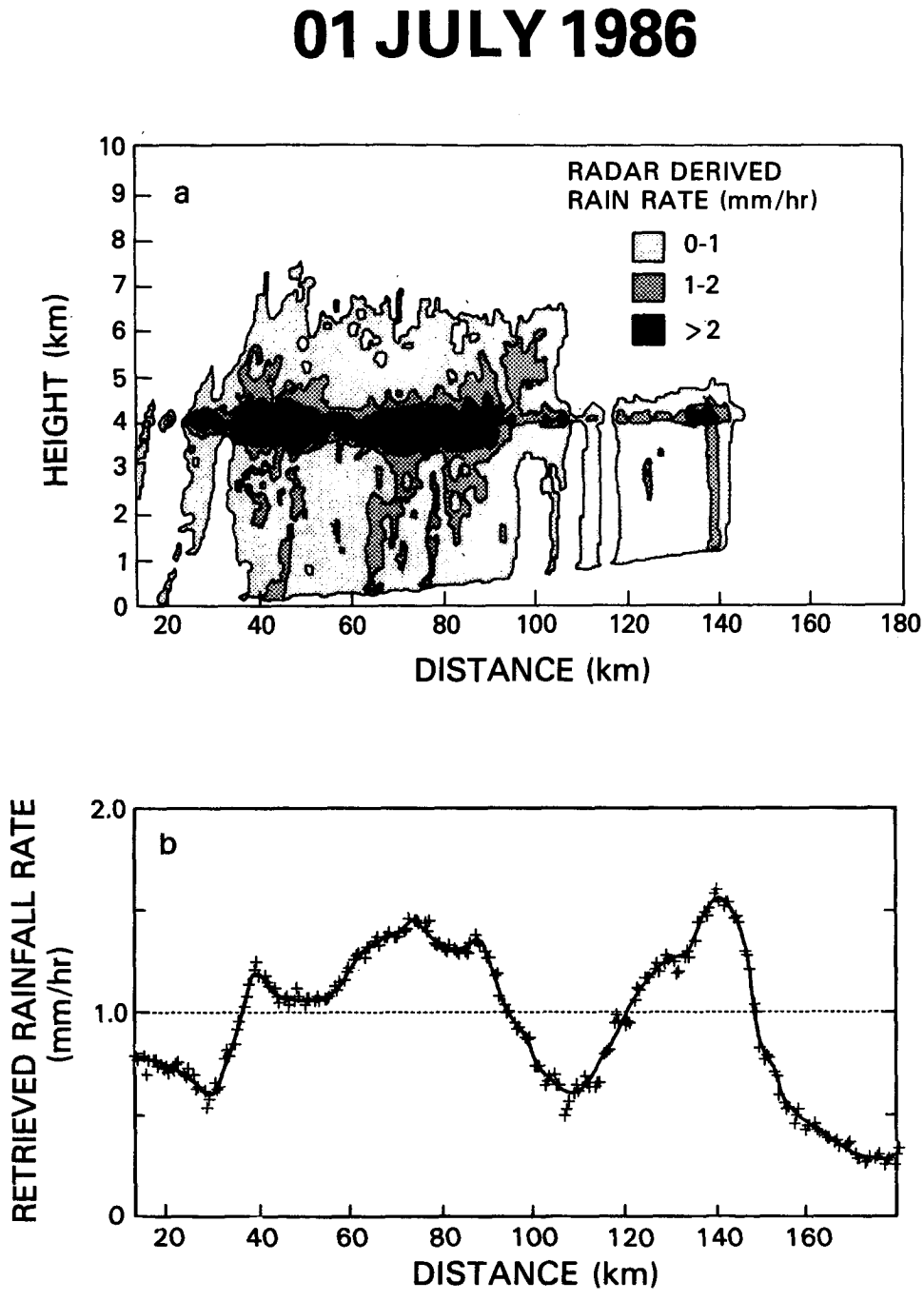

FIG. 4. Rainfall rates corresponding to the light precipitation over water off the coast of Virginia on 1 July 1986. (a) Radar-derived rainfall rates assuming Marshall–Palmer drop-size distributions for liquid up to the bright band (4 km), and ice above the bright band. (b) Retrieved surface rainfall rates deduced from the aircraft brightness temperatures shown in Fig. 3.

the rainfall rate, R_L, was allowed to vary between 0 and 20 mm h^{-1}. The cloud liquid water, Q_L, was allowed to vary between 0 and 0.7 g m^{-3}. The ocean surface temperature, T_S, was allowed to vary between 290 and 295 K, while the surface wind speed, U_0, was allowed to vary between 3 and 9 m s^{-1}. The ranges of these last two variables were commensurate with local observations. The retrieval scheme described in section 2 was used to obtain values for these four variables, which, in turn, were used as input to the cloud radiative model to generate brightness temperatures for each of the MPR channels. The procedure was repeated while varying the freezing level height and the cloud water and ice water parameterizations in order to minimize

differences between observed and retrieved brightness temperatures. The freezing level was raised and lowered by 0.5 km in successive trials, while the ice water parameterization was varied between 0.2 and 0.7 · R_L. It was found that a freezing level of 4 km produced the best results while the ice water content parameterization had little influence on the results. The final root-mean-square (rms) difference in these brightness temperatures using one cloud radiative model for the entire flight line was 4.6 K. This is small in comparison to the size of the signal produced by rain or cloud water (~50 K).

The retrieved rainfall rates along the flight line compare quite well with the radar-derived rainfall rates. An interesting observation to note is that in both the radar-derived and retrieved surface rainfall data, the rain rates from the area with the bright band (30–90 km from the radar station) and the area without the bright band (110–140 km) are similar in magnitude. Figure 3, however, reveals that the microwave T_B values in the bright band region are ~10 K colder than in the region without a bright band. One possible explanation for this difference is that the presence of the bright band is responsible for the T_B depression (due to the scattering effects of the melting ice). According to our present understanding of radiative transfer processes in the microwave regime, however, any T_B depression due to scattering must also be accompanied by a comparable decrease in the difference between horizontally and vertically polarized T_B's emerging from the surface. Due to the lack of sensitivity to the ice water content parameterization, it does not appear that the ice above the bright band itself can be responsible for this brightness temperature depression. Rather, the observations support the hypothesis that the warmer T_B values are a result of increased cloud liquid water content in the region without the radar bright band. This hypothesis would also explain the decrease in polarization difference over this bright band-free region without any corresponding increase in rainfall rate. This explanation is also consistent with the retrieved liquid water content of the cloud. Unfortunately, no in-situ measurements of cloud liquid water were made from low-altitude aircraft on this day.

b. Intense convective rain case—29 June 1986

On 29 June 1986, the ER-2 made two passes over intense convection along the North Carolina–Virginia border. Figure 5 shows the aircraft flight track used in this study superimposed on the GOES satellite visible and infrared (11 μm) imagery that coincided with the aircraft overflight. The satellite imagery shows a large anvil cloud with numerous overshooting tops over land. A minimum brightness temperature of 198 K was observed in the infrared imagery, which corresponds to a cloud top height of ~16 km when compared with the temperature profile from a nearby sounding.

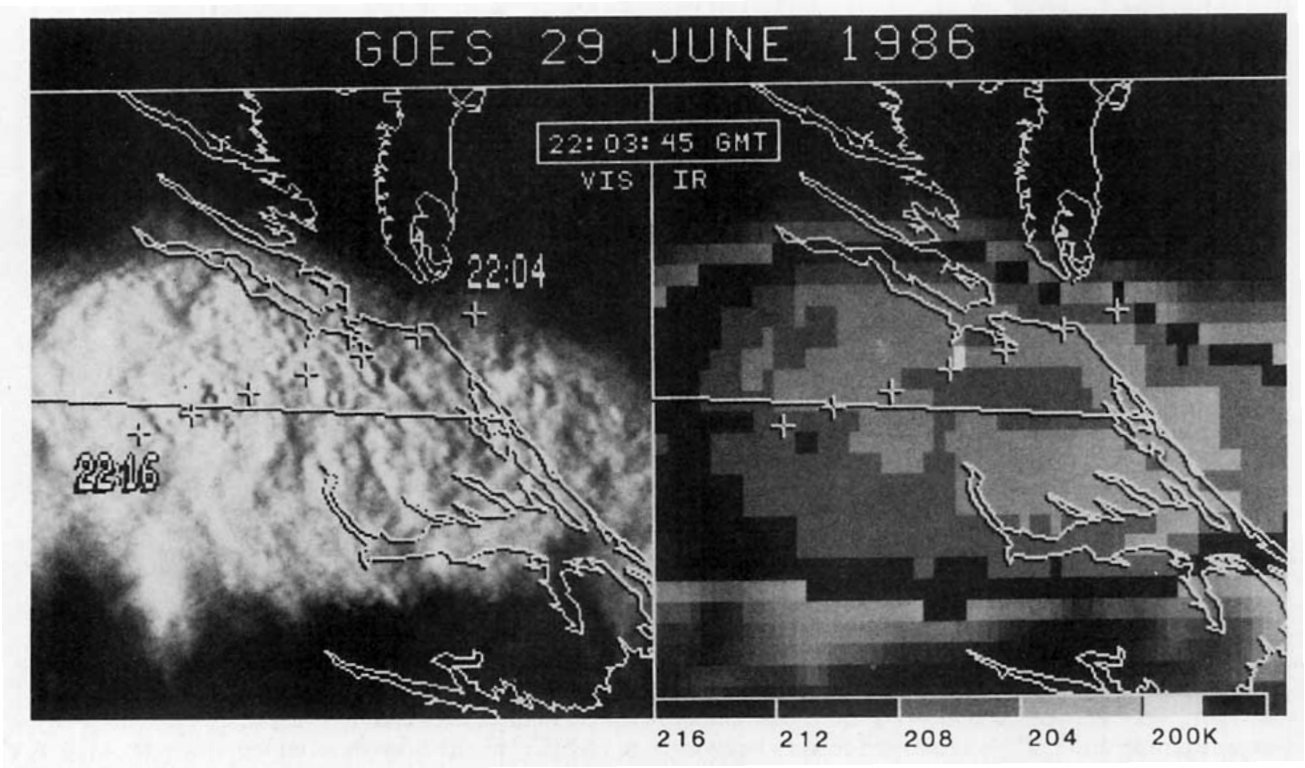

FIG. 5. VIS/IR image from GOES-East satellite showing a severe thunderstorm along the Virginia–North Carolina border on 29 June 1986. The position of the aircraft is shown superimposed on the two figures. The coldest point in the IR (198 K) corresponds to a height of ~16 km.

Figure 6 shows a 6.0 km Constant Altitude Plan Position Indicator (CAPPI) image at 2209 UTC generated from volume scans made by NASA's SPANDAR radar. Leg 1, from 2204–2214 UTC, is also plotted on the radar image. The aircraft flew along a line of cells which extended from the northeast (125 km from the radar) to the southwest (225 km from the radar). Maximum radar reflectivities of greater than 50 dBZ can be observed along this line near 2212 UTC. Intense cells can also be seen to the north of this line, but were not observed by the aircraft.

This case was representative of intense convective activity with very large rainfall rates over a land background. Since much of the microwave signature in this case represents scattering of radiation away from the radiometrically warm background, the 92 GHz channel from the AMMS instrument as well as the four channels of the MPR were included for this retrieval. Hakkarinen and Adler (1988), as well as Heymsfield and Fulton (1988), have had reasonable success delineating convection with only the 92 GHz channel. Because the AMMS scans along nadir while the 18 and 37 GHz channels on the MPR look forward at 45°, the two sensors view slightly different structures at any given time. For a given penetration depth, this difference in the viewing geometry may be expressed as a small time lag between these two datasets. In order to correct for the time lag between datasets, maximum and minimum brightness temperatures observed for features found in both the 37H GHz (horizontally polarized) and the 92 GHz channel were sampled. A regression analysis was performed relating the 37H GHz channel T_B's with a time offset from the 92 GHz T_B's. The time of the MPR observations were then adjusted to match more closely in time with the AMMS observations, effectively minimizing the time offset between

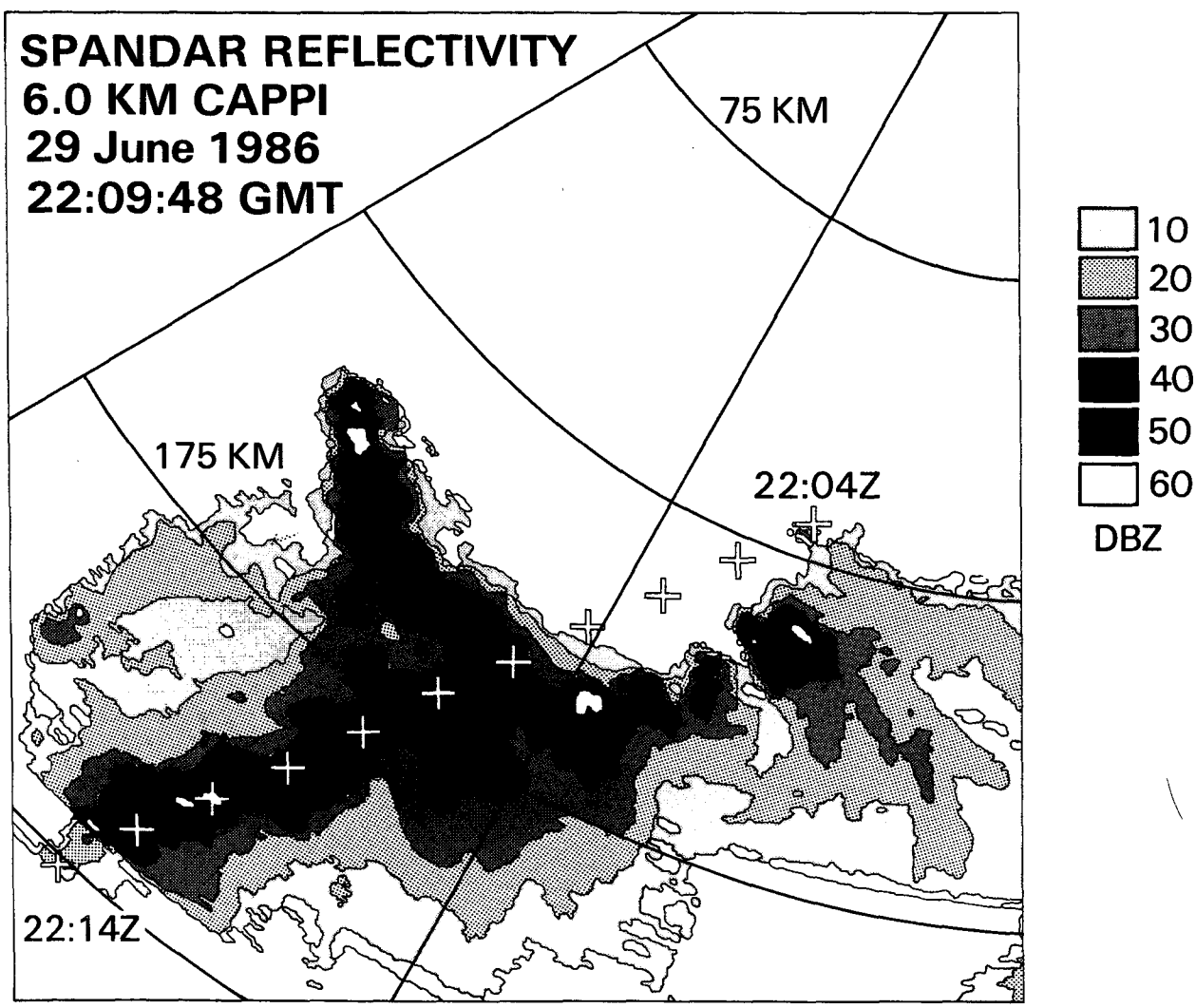

FIG. 6. SPANDAR radar representation of the 29 June 1986 thunderstorm overflown by the NASA ER-2 aircraft. The CAPPI (Constant Altitude Plan Position Indicator) represents a constant altitude cross section through the storm at 6 km. The aircraft track is superimposed on the figure.

the two datasets. Figure 7a shows a time series plot of the "adjusted" 18H (horizontal polarization), 37H, and 92 GHz temperatures along the flight track. At 92 GHz, the intense thunderstorm cores produce brightness temperatures as low as 70 K. Even at 18 GHz, a minimum of 195 K is reached. These low brightness temperatures are caused by very large concentrations of ice particles in the middle and upper parts of the thunderstorm cores. Figure 7b illustrates the brightness temperature differences between the two polarizations at 37 GHz by showing both the vertical and horizontal polarizations. This dataset was not shifted to account for differences in the viewing geometries between the MPR and the AMMS. Due to the large optical depth of these clouds, the observed differences in this case can only be attributed to the nonspherical nature of the hydrometeors.

Figure 8a shows rain rates derived from the radar vertical cross section along the flight track. Since the flight line in this case is not along a radial, the cross section was generated from volume scan data taken by the SPANDAR radar. Below the freezing level (4 km), the relation between rain rate and reflectivity given by Eq. (3) was used. The absence of a bright band, and a maximum echo height of 16 km in this case, suggests that this region is strongly convective. The relationship for ice defined in the previous section is therefore used only above 9.4 km (−35°C). The transition layer is assumed to contain hydrometeors in a mixed phase. The mixing ratio of liquid and ice is further taken to vary linearly with height.

Figure 8a shows regions of very intense rain rates along the flight path. A cell at 62.0 km along the cross section has a rain rate of greater than 80 mm h^{-1} ex-

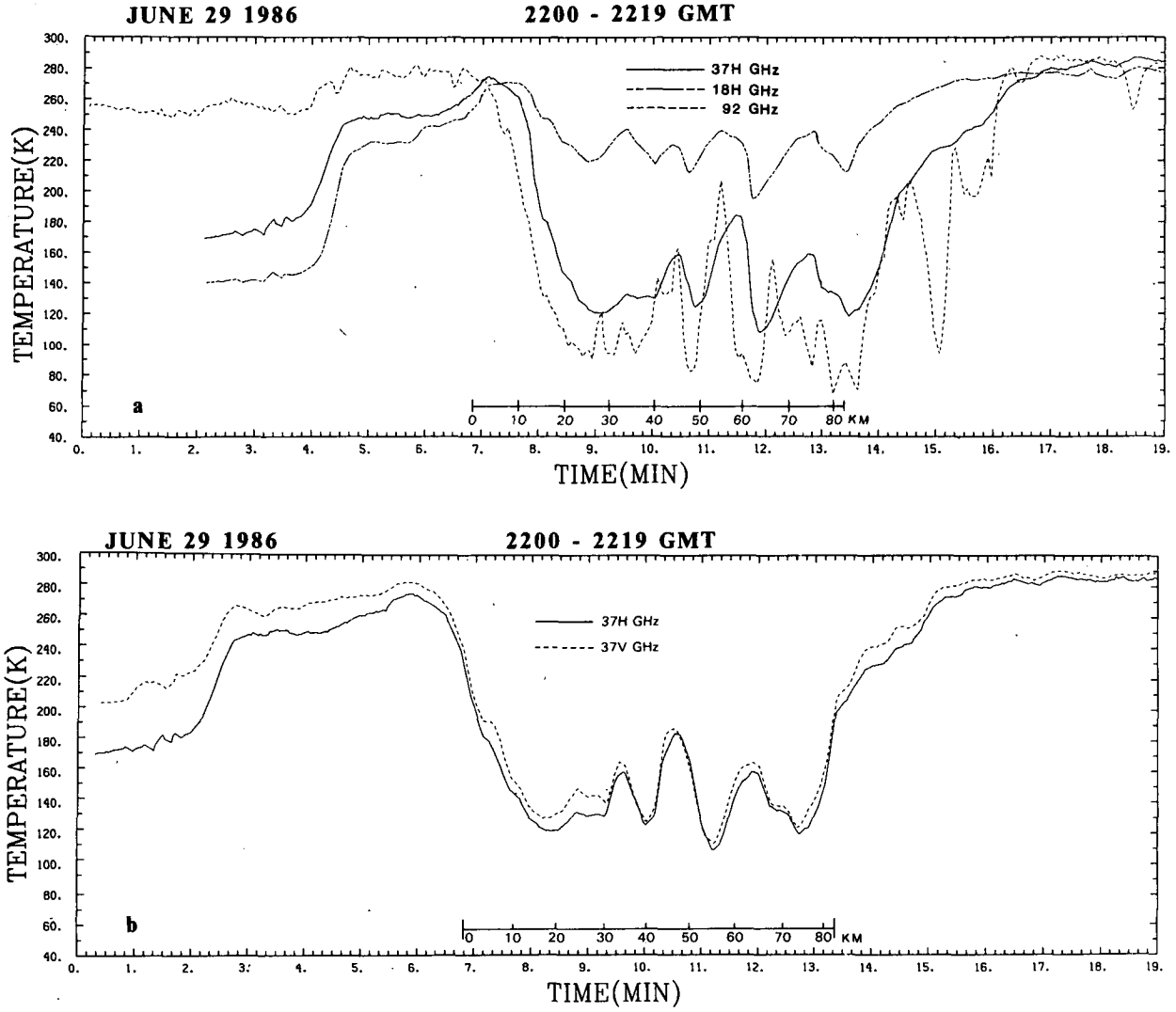

FIG. 7. Traces from passive microwave channels as the aircraft overflew thunderstorms on 29 June 1986. (a) Brightness temperature is plotted as a function of time for the 18 and 37 GHz vertical polarizations, and the 92 GHz channel. Instrument viewing offsets have been corrected so that the minimum temperatures coincide in all three channels. (b) Brightness temperatures for 37 GHz vertically and horizontally polarized channels as a function of time. Times in this figure were not corrected to minimize viewing geometry differences.

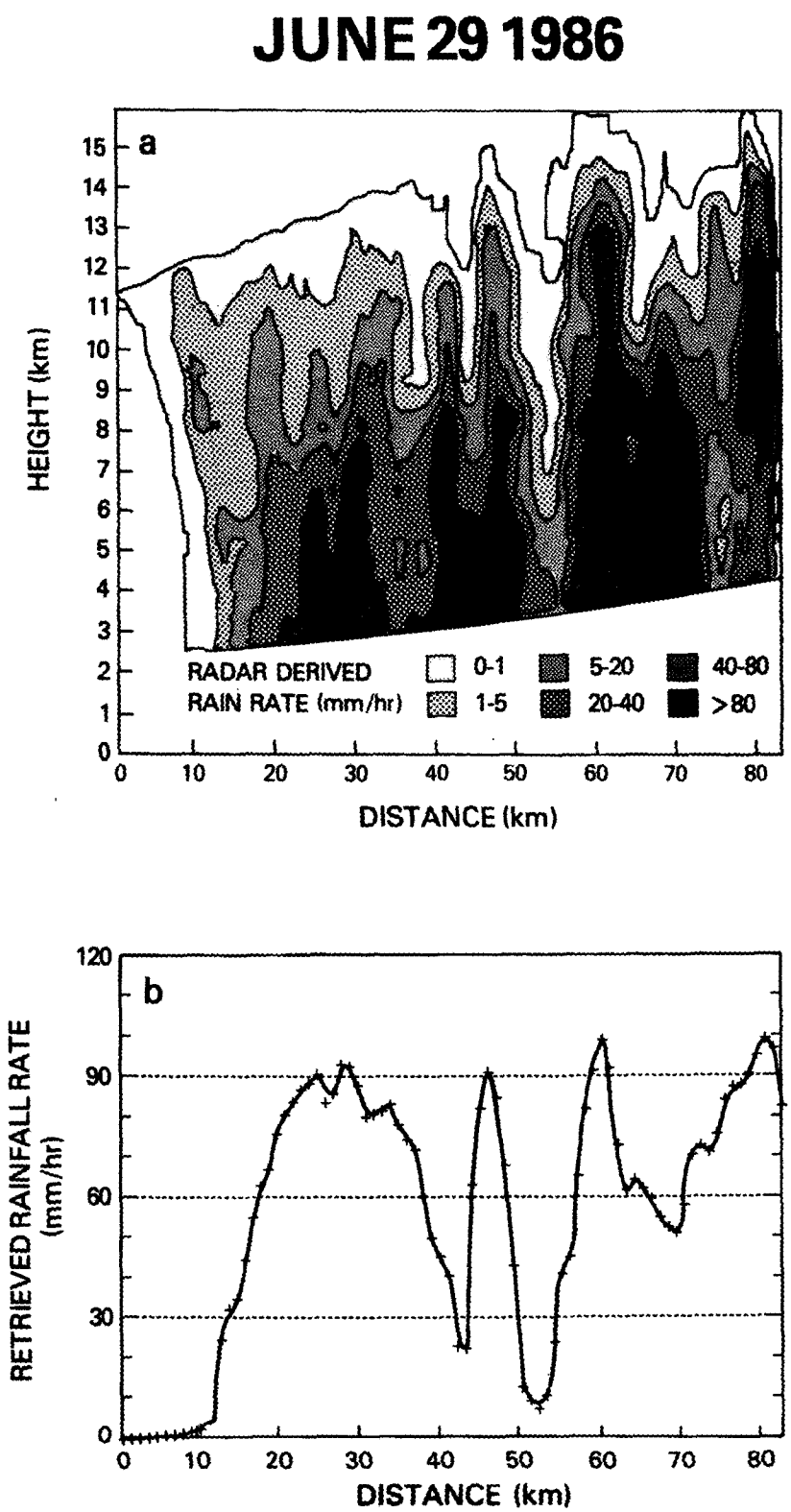

FIG. 8. Rainfall rates corresponding to the heavy precipitation associated with a severe thunderstorm along the Virginia–North Carolina border on 29 June 1986. (a) Radar-derived rainfall rates assuming Marshall–Palmer drop-size distributions for liquid up to 4 km, ice above 9.5 km, and linearly mixed hydrometeors in the transition region. (b) Retrieved surface rainfall rates deduced from the MPR brightness temperatures shown in Fig. 7a.

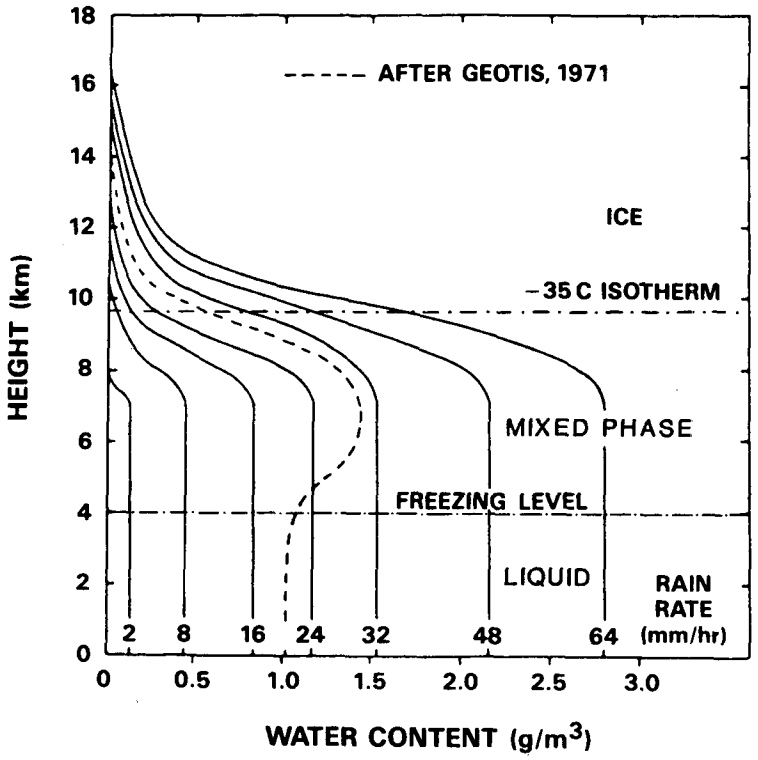

FIG. 9. Schematic model of the distribution of hydrometeors with various phases as a function of height as defined by Wu and Weinman (1984). The dashed profile is due to Geotis (1971).

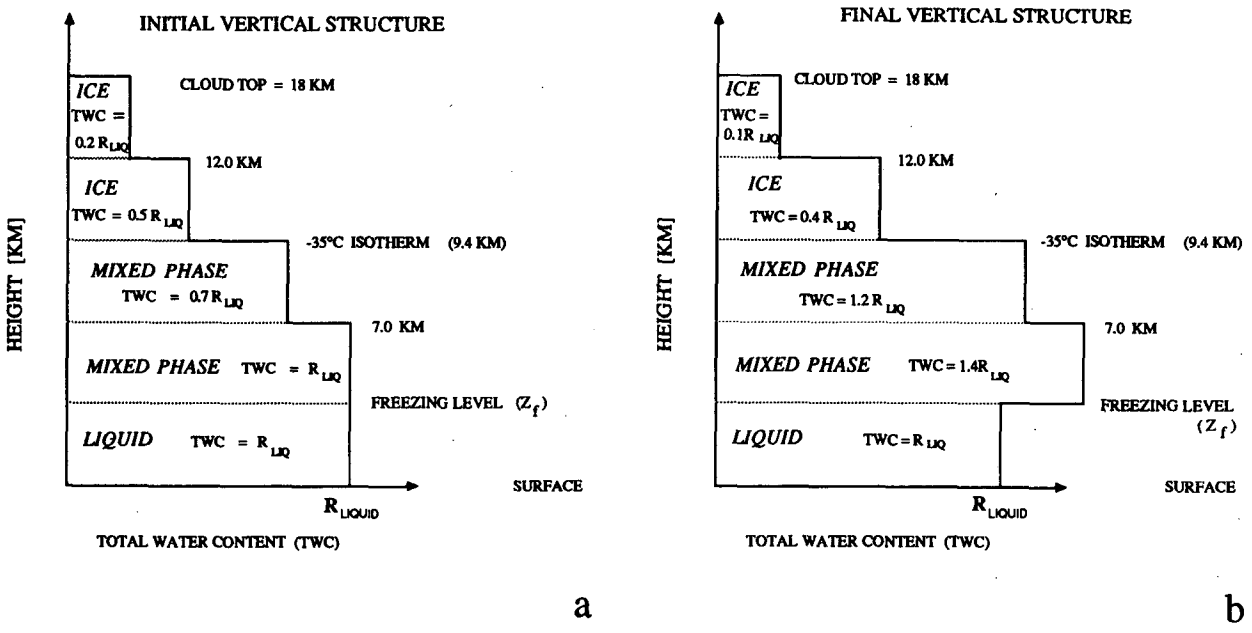

FIG. 10. Schematic model of the distribution of hydrometeors with various phases as a function of height in the five layer cloud model. (a) Five layer representation of the profile defined by Wu and Weinman shown in Fig. 9. (b) Five layer representation of the vertical hydrometeor distribution best suited for the retrieval of rainfall for the 29 June case study (strong convective region).

tending to ~10 km. Comparisons can be made between the radar cross section (Fig. 8a) and the time series plot (Fig. 7a). For instance, at 55 km along the radar cross section is a region of low rainfall rates between two intense convective cells. This feature matches the increase in microwave T_B's at 2211:10 UTC between depressions at 2210:40 and 2211:50 UTC.

The parameterization of the vertical distribution of hydrometeors within the storm described by Wu and Weinman (1984) was initially selected as representative of convective cores. The hydrometeor structure is shown in Fig. 9. The hydrometeors are assumed liquid from the surface to the freezing level, in a combined phase up to the −35°C isotherm, and all ice above this level. The lapse rate is assumed to be that of the U.S. Standard Atmosphere. Since the cloud radiative model used in this study is limited to five layers, the parameterization scheme of Wu and Weinman was further simplified. The initial five layer parameterization of the vertical hydrometeor structure is shown in Fig. 10a. It should be stressed, however, that the Wu and Weinman parameterization shown in Fig. 10a is only an initial guess and makes no assumptions regarding the actual cloud structure. The first layer, from the surface to the freezing level (4 km), was assumed to contain precipitable water, R_L, and cloud liquid water, Q_L. The second and third layer are assumed to contain both liquid and frozen hydrometeors, the ratio of which varies linearly between the freezing level and the top of the third layer (9.4 km). Since the layers are assumed to be homogeneous, the average layer height must be used to determine the specific ratio of liquid to ice in each of the two layers. The second layer extends vertically to a height of 7 km, and contains total precipitable water (both liquid and ice), R_T, equal to the liquid in the layer below (R_L). The cloud liquid water in this layer was assumed to be $0.5Q_L$. The third layer, extending from 7 km to the −35°C isotherm (9.4 km) contains total precipitable water $R_T = 0.7R_L$, and a cloud liquid water content of $0.2Q_L$. The ice water content, IWC, in the second and third layer can be obtained from IWC = R_T(layer)*[9.4 − Z_{av}(layer)]/5.4 km. The fourth and fifth layers were assumed to contain only ice in amounts of $0.5R_L$ and $0.2R_L$, respectively.

The optical thickness of the rain and clouds in this case is quite large, effectively obscuring the Earth's surface and implying that changes in the surface temperature, T_S, and emissivity, ϵ, do not significantly affect the upwelling T_B's observed by the radiometers. These parameters were therefore held constant at T_S = 298 K, and ϵ = 0.9 for all frequencies. Nonetheless, a large number of parameters can be varied in this model. Because the upwelling brightness temperatures are very sensitive to the vertical structure of hydrometeors, care must be taken to find the most representative structure. Total water content (TWC) of the surface layer is allowed to vary freely. The TWC in the upper layers, however, as well as the thickness of each layer and the ratio of ice in the mixed phase layers, was parameterized in terms of the TWC of the surface layer in the cloud radiative model. The structure which provided optimal agreement between observed and retrieved brightness temperatures was obtained by changing first the TWC parameterization in the upper layers and then the ratios of ice to liquid in each mixed phase layer. It was found that the layer thickness, as well as the TWC and the ratio of ice to liquid water had measurable effects on the retrieved results.

The final vertical hydrometeor structure of the cloud in the five layer model is shown in Fig. 10b. Comparison with Fig. 9 indicates that the final structure of the rain better resembles the structure described by Geotis (1971) (cf. Fig. 9, dashed curve) than the initial guess (Fig. 10a). Examination of the radar-derived rain rates also reveals that the final cloud structure better resembles the actual cloud structure than the initial guess. The corresponding optimal rainfall result is shown in Figure 8b. The rms difference between the observed and retrieved brightness temperatures in this case is 14.7 K. This is large compared to the 1 July study, but is still small with respect to the magnitude of the signal produced by the precipitation (~150 K) in this case. Furthermore, some of the largest errors for 29 June stem from regions where the slope of the brightness temperature profiles was very steep. Since these data were corrected to account for the time lag between the 92 GHz channel and the lower frequencies of the MPR, errors in these regions are not particularly troublesome. Agreement in the regions not significantly affected by the time lag correction (all but the steep slope regions) have smaller average errors (~12°K).

5. Potential applications to satellite retrievals

Satellite retrievals differ from the aircraft retrievals only in their spatial resolution. The SSM/I aboard the DMSP satellite, flying in an 833 km polar orbit, samples data every 25 km for the 19, 22 and 37 GHz channels, and every 12.5 km for the 85 GHz channel (Hollinger et al. 1987). The proposed TRMM satellite (Simpson et al. 1987), flying in a low-inclination, low-altitude orbit (~300 km), would have resolutions of 10 km for the low frequency channels and 3 km for the 85 GHz channel. Footprints for the SSM/I are roughly 100 times the size of the aircraft sensor footprints, while the TRMM sensor footprints would be roughly 10 times larger than the aircraft sensor footprints.

In the subsequent study, an imaginary satellite measuring dual-polarized brightness temperatures at 18, 37 and 85 GHz with uniform ground resolution of 20 km is considered. Satellite-observed brightness temperatures will be simulated by randomly selecting a rainfall rate, the fraction of the footprint filled by the rain, and the nonprecipitating liquid water content of the cloud. Although the precipitating cloud is allowed to only partially cover the satellite field of view, the nonprecipitating cloud water will be assumed to be

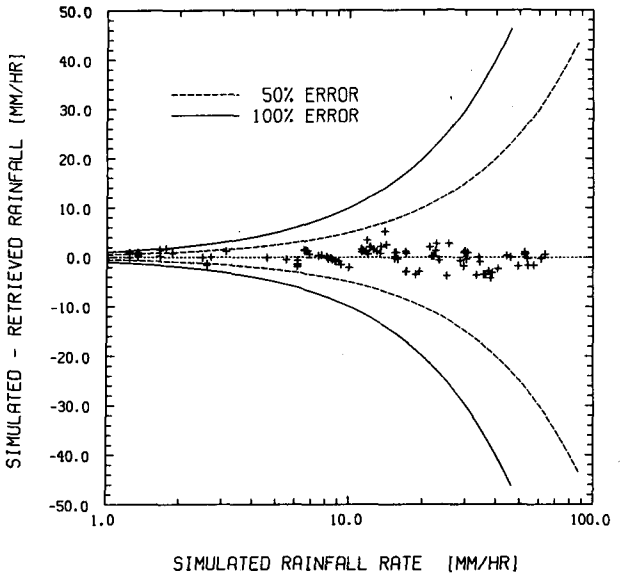

FIG. 11. Differences between the simulated footprint-averaged rainfall rate and retrieved rainfall rate as a function of simulated rainfall rate. Satellite footprints were assumed to be 20 × 20 km, with random fractions covered by rain. Satellite T_B's were simulated using the parameterization shown in Fig. 10b. Regression statistics were generated using the same vertical hydrometeor structure parameterization used to simulate satellite observations.

homogeneously distributed throughout the entire footprint. Convective precipitating cores over land are simulated, with the vertical structure of such storms given by the best fit obtained in the previous section (Fig. 10b). Surface temperature is allowed to vary randomly within an 8°K range (i.e., $T_S = 292 \pm 4$ K), and the emissivity over land will be allowed to vary between 0.8 and 0.95. Although the emissivity is assumed constant with frequency, its large range is used to represent the naturally occurring variability of this parameter. Finally, in order to make these simulations as realistic as possible, random noise of ±2°K is added to the simulated brightness temperatures.

With the simulated parameters serving as ground truth for the following study, the statistical technique used to retrieve rain rates from the aircraft data is applied to the simulated satellite data. Results which can be obtained if the vertical cloud structure used to simulate satellite data is also used to generate the retrieval statistics are shown in Fig. 11. The same assumptions about the surface temperature and emissivity used to simulate brightness temperatures are also used here. As can be seen from the figure, the retrieved rainfall is in excellent agreement with the simulated rainfall for all but the lightest rainfall rates. This is not too surprising, since the small signatures associated with light rain over land are easily masked by the highly variable surface characteristics. Also noteworthy is the absence of any bias in the result. This is important if one is interested in large area averages which are not very sensitive to these small individual errors as long as the results are not biased. Finally, it should be noted that the difference between the simulated and retrieved brightness temperatures in this example is only 2.3°K, which is very small considering the random noise of ±2°K added to the simulated data. The excellent agreement between simulated and retrieved rainfall rate is artificially good, however, because the cloud vertical structure is exactly reproduced, and the physics of radiative transfer is the same for both simulated data and the retrieval statistics.

Incomplete knowledge of the cloud vertical structure is assumed for a second example. This retrieval is performed using the five-layer simplification of the convective core model of Wu and Weinman (1984) to generate statistics (Fig. 10a). This structure, although similar to the structure used to simulate the data, might be a reasonable guess in the absence of detailed cloud structure information. Results for this retrieval are shown in Fig. 12. It is noteworthy that the retrieved rainfall rates in this study are, in general, slightly lower than the simulated ones. The disagreement between simulated and retrieved brightness temperatures, however, has also increased from 2.3° to 2.5°K, indicating that this is probably not the best possible cloud structure with which to do retrievals in this particular instance. In reality, however, this 0.2° K difference is too small to differentiate between the two cloud structures used in the retrieval procedure. Alternately, the two retrieval procedures must be considered equivalent, even if one introduces small biases into the retrieved rainfall for this set of simulated observations.

As a final example, the effect of using a very simple stratiform cloud model to generate statistics is investigated. For this example, the cloud vertical structure is assumed to consist of only two layers: a liquid surface layer and a frozen layer of variable thickness above the

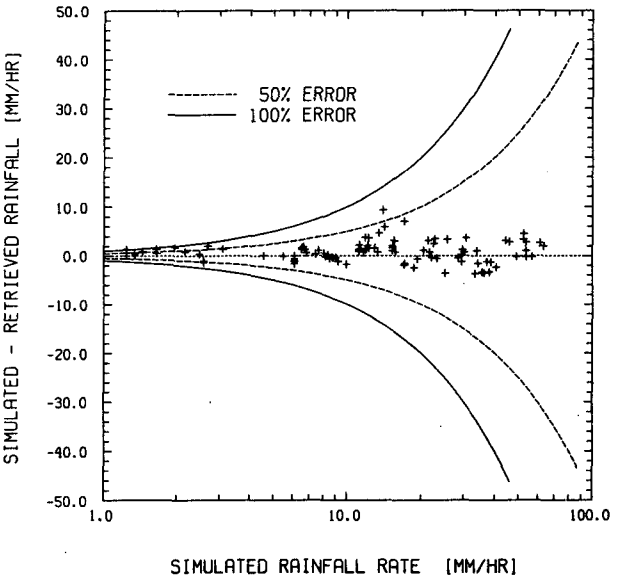

FIG. 12. As in Fig. 11, but regression statistics were generated using the five-layer parameterization of Wu and Weinman (1984) shown in Fig. 10a.

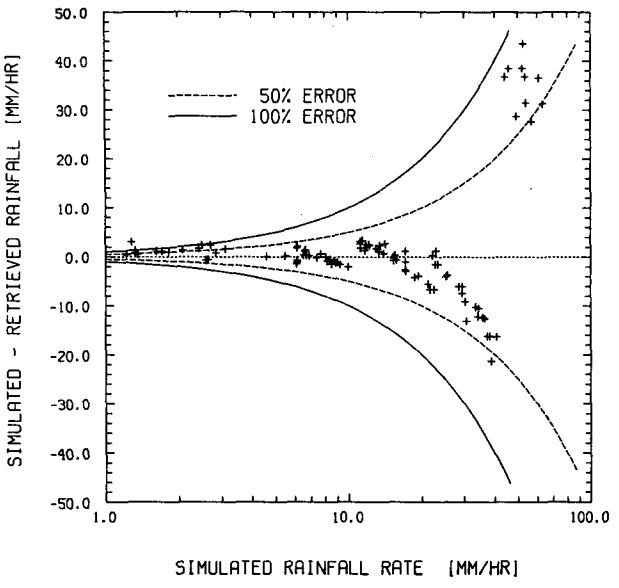

FIG. 13. As in Fig. 11, but regression statistics were generated using a two-layer model containing liquid in the bottom layer, and having a layer of variable thickness above the freezing level containing all ice.

freezing level containing the same total water content as that of the liquid layer. The surface characteristics will still be those assumed for the simulated data. Results of this retrieval are shown in Fig. 13. As can be seen in this figure, the retrieval errors are now quite large, overestimating the simulated rainfall in the moderate rainfall range, and underestimating the rainfall at the high rainfall rates. The disagreement between observed and simulated brightness temperatures for this example, however, is 13.1°K, indicating that this cloud model is a much poorer choice for the interpretation of the simulated data than were the previous two examples. The overestimate of retrieved rain rates for rainfalls less than 40 mm h^{-1} is probably due to the fact that the 2-layer model used in this particular retrieval scheme has less ice in it for a given rainfall rate than does the 5-layer model used to generate the simulated brightness temperatures. This implies that extra hydrometeors must be added to the profiles by the retrieval scheme in order to reproduce the simulated brightness temperatures. Above 40 mm h^{-1}, the fact that the 2-layer model of this retrieval does not consider mixed phase layers seems to become important, producing brightness temperatures which are too low at the simulated rain rates. Thus the retrieval procedure selects profiles with somewhat fewer hydrometeors, producing the observed underestimate of rainfall rates. The sharp discontinuity at 40 mm h^{-1} is an artifact of the piecewise linear regression scheme used. Rain rate intervals 5 and 6 correspond to 20–40 mm h^{-1} and 40–100 mm h^{-1}, respectively. The discontinuity in the retrieved rain rate at 40 mm h^{-1} is a result of the discrete steps between these intervals. Table 1 presents a more quantitative comparison of the errors in the retrieved rainfall and the disagreements between simulated and retrieved brightness temperatures for each of the three cloud structures used in generating retrieval statistics. Most of the retrievals found to contain excessive errors (>50%) are clearly identified by large disagreements between simulated and retrieved T_B's. The question of uniqueness of the solutions, however, is not easily answered, due to the statistical nature of the retrieval.

6. Conclusions

The method for rainfall retrievals described here offers the possibility of generating high quality retrievals when high resolution data such as that obtained from aircraft radiometers are used. Results shown here for two very distinct rainfall conditions both agree with the radar-derived surface rainfall rates to within the accuracy of the radar measurements. Further improvements of this rainfall retrieval scheme will have to be tested using a network of raingages and more carefully calibrated radar systems.

The technique also offers the possibility of deducing some information about the hydrometeor distribution within the precipitating clouds. This may become very important if space-borne radars, which can probe the vertical structure of clouds, are to be used in the near future. Techniques using a combination of radar and radiometer data may become very powerful by requiring consistency between the various retrieved parameters, or by using radiometric and radar results iteratively to determining the cloud vertical hydrometeor profiles.

Finally, using simulated satellite observations, this technique was successfully applied to simulated satellite data. While the total information available from satellite data is less than that of aircraft radiometric observations, and disagreement between retrieved and observed brightness temperatures is likely to be larger than those obtained with simulated data due to the uncertainties associated with real data, this technique should prove very useful once well-calibrated surface data are available for comparison with coincident data from satellite sensors such as the SSM/I.

Because of the large rate of data collection, and the need for timely output, satellite retrieval algorithms

TABLE 1. Error analysis showing the differences between simulated and retrieved brightness temperatures for the three cases described in section 5.

Error in retrieved rain rate	Case 1		Case 2		Case 3	
	No. of obs.	ΔT_B (°K)	No. of obs.	ΔT_B (°K)	No. of obs.	ΔT_B (°K)
0%–10%	45	2.2	42	2:8	21	4.6
10%–25%	30	2.2	27	2.5	28	5.4
25%–50%	4	2.5	9	2.4	19	10.6
50%–100%	0	—	1	4.3	11	70.8
>100%	0	—	0	—	0	—

also require that the retrieval procedure be computationally fast. While the procedure described here has some common elements with variational techniques, such as that of Olson (1986), its statistical nature tends to obscure some of the physics in exchange for computational efficiency. One advantage of using a statistical approach is that once a cloud radiative model is adjusted to a specific rain condition, that model can be used for scenes much larger than individual footprints as long as the cloud model parameters (independent of the free parameters) remain homogeneous. Although this is largely the case for the two flight lines examined in this study, it is unclear whether it will be true for convective regions when examined with the much coarser resolution available from space-borne radiometers. At worst, however, this scheme is equivalent to physical retrieval approaches which incorporate no information from neighboring pixels.

Operational retrieval techniques cannot, due to the large data collection rates, depend on interactive schemes to produce rainfall estimates. For operational applications, it will therefore be necessary to preselect a number of cloud models. Rather than interactively selecting the cloud model which minimizes the differences between observed and retrieved brightness temperatures, it will be necessary to try all models simultaneously, and then choose the one that produces the smallest differences in the brightness temperatures. At present, each cloud model requires ~2 seconds of CPU time on a VAX11/780. Faster CPUs, along with parallel-processing software to handle the distinct cloud models, should result in acceptable computation times.

Acknowledgments. The authors would like to thank Dr. Robert Adler for his continuing support of the aircraft microwave studies. Drs. J. Weinman, J. Simpson, G. Heymsfield and M. Yeh provided many helpful suggestions in the preparation of this manuscript. This research was supported by NASA's Mesoscale Atmospheric Processes Research Program.

REFERENCES

Adler, R. F., W.-K. Tao, N. Prasad, J. Simpson and H.-Y. Yeh, 1988a: Satellite microwave rainfall simulations with a three-dimensional dynamical cloud model. Preprints, *Third Conf. Satellite Meteorology and Oceanography,* Anaheim, CA, Amer. Meteor. Soc., 290–295.

——, N. Prasad, W.-K. Tao, H.-Y. Yeh, R. Mack and J. Simpson, 1988b: Microwave observations and modeling of deep convection. *Tropical Rainfall Measurements,* J. S. Theon and N. Fugono, Eds., A. Deepak, 185–191.

——, W.-K. Tao, N. Prasad, J. Simpson and H.-Y. Yeh, 1988: Satellite microwave rainfall simulations with a three-dimensional dynamical cloud model. Preprints, *Third Conf. Satellite Meteorology and Oceanography,* Anaheim, CA, Amer. Meteor. Soc., 290–295.

Chang, A. T. C., and A. S. Milman, 1982: Retrieval of ocean and atmospheric parameters from multichannel microwave radiometric measurements. *IEEE Trans. Geosci. Remote Sens.,* **20,** 217–224.

Dodge, J., J. Arnold, G. Wilson, J. Evans and T. Fujita, 1986: The Cooperative Huntsville Meteorological Experiment. *Bull. Amer. Meteor. Soc.,* **67,** 417–419.

Evans, B. G., and A. R. Holt, 1977: Scattering amplitudes and cross polarization of ice particles. *Electon. Lett.,* **13,** 342–344.

Geotis, S. G., 1971: Thunderstorm water contents and rain fluxes deduced from radar. *J. Appl. Meteor.,* **10,** 1233–1237.

Hakkarinen, I. M., and R. F. Adler, 1988: Observations of convective precipitation at 92 and 183 GHz: aircraft results. *Meteor. and Atmos. Phys.,* **38,** 164–182.

Heymsfield, G. M., and R. Fulton, 1988: Comparison of high-altitude remote aircraft measurements with the radar structure of an Oklahoma thunderstorm: implications for precipitation estimation from space. *Mon. Wea. Rev.,* **116,** 1157–1174.

Hollinger, J., R. Lo, G. Poe, R. Savage and J. Pierce, 1987: *Special Sensor Microwave/Imager User's Guide,* Naval Research Laboratory, Washington, D.C., 120 pp.

Huang, R., and K.-N. Liou, 1983: Polarized microwave radiation transfer in precipitating cloudy atmospheres: application to window frequencies. *J. Geophys. Res.,* **88,** D3885–3893.

Kummerow, C., 1987: Microwave radiances from horizontally finite, vertically structured clouds. Ph.D. thesis, Univ. of Minnesota, Minneapolis, 146 pp.

——, and J. A. Weinman, 1988: Determining microwave brightness temperatures from horizontally finite and vertically structured clouds. *J. Geophys. Res.,* **93,** D3720–3728.

Marshall, J. S., and W. M. Palmer, 1948: The distribution of raindrops with size. *J. Meteor.,* **5,** 165–166.

Oguchi, T., 1983: Electromagnetic wave propagation and scattering in rain and other hydrometeors. *Proc. IEEE,* **71,** 1029–1078.

Olson, W. S., 1986: Model-based retrieval of tropical cyclone rainfall rates using the Nimbus-7 SMMR. Preprints, *Second Conf. Satellite Meteorology/Remote Sensing and Applications,* Williamsburg, VA, Amer. Meteor. Soc., 438–443.

——, 1987: Estimation of rainfall rates in tropical cyclones by passive microwave radiometry. Ph.D. thesis, Univ. of Wisconsin, Madison, 282 pp.

Ramana Murty, B. V., A. K. Roy and K. R. Biswas, 1965: Radar echo intensity below the bright band. *J. Atmos. Sci.,* **22,** 91–94.

Simpson, J., R. F. Adler and G. North, 1988: A proposed tropical rainfall measuring mission (TRMM) satellite. *Bull. Amer. Meteor. Soc.,* **69,** 278–295.

Smith, P. L., 1984: Equivalent radar reflectivity factors for snow and ice particles. *J. Climate Appl. Meteor.,* **23,** 1258–1260.

Spencer, R. W., 1986: A satellite passive 37 GHz scattering-based method for measuring oceanic rain rates. *J. Climate Appl. Meteor.,* **25,** 754–766.

——, W. S. Olson, R. Wu, D. W. Martin, J. A. Weinman and D. A. Santek, 1983: Heavy thunderstorms observed over land by the Nimbus-7 scanning microwave radiometer. *J. Climate Appl. Meteor.,* **122,** 1041–1046.

Szejwach, G., R. F. Adler, I. Jobard and R. A. Mack, 1986: A cloud model–radiative model combination for determining microwave T_B-rain rate relations. Preprints, *Second Conf. Satellite Meteorology/Remote Sensing and Applications,* Williamsburg, VA, Amer. Meteor. Soc., 444–449.

Tao, W.-K., and J. Simpson, 1984: Cloud interactions and merging: Numerical simulations. *J. Atmos. Sci.,* **41,** 2901–2917.

——, J. Simpson and S.-T. Soong, 1987: The statistical properties of a cloud ensemble: A numerical study. *J. Atmos. Sci.,* **44,** 3175–3187.

Weinman, J. A., and P. J. Guetter, 1977: Determination of rainfall distribution from microwave radiation measured by the Nimbus-6 ESMR. *J. Appl. Meteor.,* **16,** 437–442.

Wilheit, T. T., J. L. King, E. B. Rodgers, R. A. Nieman, B. M. Krupp, A. S. Milman, J. S. Stratigos and H. Siddalingaiah, 1982: Microwave radiometric observations near 19.35, 35, 92 and 183 GHz of precipitation in tropical storm Cora. *J. Appl. Meteor.,* **16,** 551–560.

Wu, R., and J. A. Weinman, 1984: Microwave radiances from precipitating clouds containing aspherical ice, combined phase, and liquid hydrometeors. *J. Geophys. Res.,* **89,** 7170–7178.